Layered $LiNi_{0.5}Co_{0.5}O_2$ cathode materials grown by soft-chemistry via various solution methods

C. Julien[a,] C. Letranchant[a], S. Rangan[a], M. Lemal[a], S. Ziolkiewicz[a], S. Castro-Garcia[b], L. El-Farh[c], M. Benkaddour[c]

a Laboratoire des Milieux Désordonnés et Hétérogènes, UMR7603, Université Pierre et Marie Curie, 4 place Jussieu, 75252 Paris, Cedex 05, France

b Departamento Quimica Fundamental e Industrial, Universidade A Coruna, 15071 A Coruna, Spain

c Laboratoire d'Analyse et Caractérisation des Matériaux, Université Mohamed 1er, Faculté des Sciences, Oujda, Morocco

Materials Science and Engineering: B

Volume 76, Issue 2, 3 July 2000, Pages 145–155

Received 2 November 1999, Revised 8 February 2000, Accepted 17 February 2000, Available online 30 May 2000

doi:10.1016/S0921-5107(00)00431-1

Abstract

The lithiated nickel–cobalt oxide $LiNi_{0.5}Co_{0.5}O_2$ used as cathode material was grown at low-temperature using different aqueous solution methods. The wet chemistry involved the mixture of metal salts (acetates or nitrates) with various carboxylic acid-based aqueous solutions. Physicochemical and electrochemical properties of $LiNi_{0.5}Co_{0.5}O_2$ products calcined at 400–600°C were extensively investigated. The four methods used involved complexing agents such as either citric, oxalic, aminoacetic

(glycine), or succinic acid in aqueous medium which functioned as a fuel, decomposed the metal complexes at low temperature, and yielded the free impurity $LiNi_{0.5}Co_{0.5}O_2$ compounds. Thermal (TG–DTA) analyses and XRD data show that powders grown with a layered structure ($R\bar{3}m$ space group) have been obtained at temperatures below 400°C by the acidification reaction of the aqueous solutions. The local structure of synthesized products was characterized by Fourier transform infrared (FTIR) spectroscopy. The electrochemical properties of the synthesized products were evaluated in rechargeable Li cells using a non-aqueous organic electrolyte (1 M $LiClO_4$ in propylene carbonate, PC). The $LiNi_{0.5}Co_{0.5}O_2$ positive electrodes fired at 600°C exhibited good cycling behavior.

Keywords

$LiNi_{0.5}Co_{0.5}O_2$; Rechargeable Li cell; Wet chemistry; Carboxylic acids

1. Introduction

In recent years, there has been a great deal of interest in preparation of polycrystalline materials, particularly oxides using low-temperature (LT) techniques. LT-crystallized lithiated transition-metal oxides, especially $LiMn_2O_4$, which showed some promise in improving the cycle life of rechargeable lithium batteries, have been grown by new synthesis routes such as sol–gel, combustion, and precipitation methods using complexing agents like succinic, oxalic, malic or tartaric acids [1], [2], [3], [4], [5], [6],[7] and [8]. Recently, Pereira-Ramos has critically discussed the impact afforded by LT techniques especially sol–gel synthesis and precipitation techniques on the electrochemical behavior of the oxide materials as prepared [9]. Solution preparative techniques allow a better mixing of the elements and thus a better reactivity of the mixture to obtain purer reaction products. Lower reaction temperature and shorter reaction time are then possible to yield a compound of high homogeneity and high specific area. Moreover, these LT methods make use of lower calcination temperatures resulting in particles of smaller size and a highly strained lattice.

From a technological point of view, lithiated transition-metal oxides with a layered, α-$NaFeO_2$ type, structure such as $LiMO_2$ (M=Ni and Co) have been extensively studied this last decade such as positive electrode materials for rechargeable lithium batteries.

$LiCoO_2$ has been proposed as cathode for lithium battery by Mizushima et al. in 1980 [10]. Two battery companies have demonstrated that the concept of Li-ion cell could work, on either in D, AA, or coin-sized cells based on the following electrochemical chains $LiCoO_2$/el-Li^+/carbon, $LiNiO_2$/el-Li^+/carbon, and $LiNi_{0.2}Co_{0.8}O_2$/el-Li^+/carbon systems, respectively, where el-Li^+ is a non-aqueous electrolyte [11], [12], [13] and [14].

Layered lithium transition-metal oxides (LTMOs) such as lithium cobaltate and lithium nickelate are the most advanced studied electrode materials [15] and [16]. Some limitations due to its expensive technology, toxicity, cycle life failure, and coexistence of two phases are a debatable subject in using $LiCoO_2$. There are difficulties to prepare $LiNiO_2$ in a reproducible way due to its tendency to non-stoichiometric growth, and its strong activity in the electrochemically formation of nickel dioxide at low lithium content induces an organic electrolyte oxidation and an exothermic reaction. Voltages in excess of 4 V occur for low lithium contents making LTMO cathodes highly oxidizing and are therefore, unstable in many of the organic-based electrolytes that are utilized in lithium cells [17]. To alleviate the above disadvantages, many attempts have been made to improve the lithium insertion properties by partial substitution of Co or Ni. The most well documented approach is the solid solution $LiNi_{1-y}Co_yO_2$ series [15], [16], [17], [18], [19], [20], [21], [22],[23], [24], [25], [26], [27], [28], [29], [30] and [31]. Table 1 lists the various $LiNi_{0.5}Co_{0.5}O_2$ cathode materials with their crystallographic parameters reported in the literature. $LiNi_{1-y}Co_yO_2$ compounds are isostructural with the layered oxide end-compounds. They exhibit electrochemical features with lower insertion potentials compared with that for the pure cobalt oxide phase, $LiCoO_2$. Therefore, $LiNi_{1-y}Co_yO_2$compounds were expected to be oxidatively less demanding on the electrolyte phase and to exhibit good lamellar structure. With increasing cobalt content, the trigonal distortion of the crystal lattice increases and the deviation from the stoichiometry of lithium nickelate decrease.

In this paper, we report the low-temperature synthesis of $LiNi_{0.5}Co_{0.5}O_2$ electrode materials using various aqueous carboxylic acid-assisted methods. Preparation methods consist of an acidification reaction using an organic (carboxylic) acid. Here, the complexing agent acts as a fuel during the formation process of transition-metal oxide powders. The carboxylic acid groups present in the complexing agent could form a chemical bond with the metal ions and form viscous resins on evaporation of the solvent, which are usually known as precursors. The physical properties (i.e. formation temperature, structure, local environment) of synthesized materials have been investigated by different techniques like TG–DTA, XRD and Fourier transform infrared

(FTIR). The LT procedures provide microcrystalline, layered structured $LiNi_{0.5}Co_{0.5}O_2$compounds with uniform submicron-sized particles. The electrochemical performance of these oxides has been studied by coupling them as cathodes with Li anodes and a non-aqueous electrolyte mixture.

Table 1.

Synthesis and crystallographic parameters of $LiNi_{0.5}Co_{0.5}O_2$ compounds

Synthesis	*a* (Å)	*c* (Å)	*c*/*a*	References
Li_2CO_3+$CoCO_3$+$NiCO_3$, 850°C	–	–	–	[22]
Li_2CO_3+$CoCO_3$+$NiCO_3$, 850°C	–	–	–	[23]
Li_2CO_3+$CoCO_3$+$NiCO_3$, 650°C	2.844	14.126	4.930	[17]
Li_2CO_3+$NiCO_3$+$CoCO_3$, 700/900°C	2.839	14.094	4.964	[24]
Electron-beam evaporation	2.85	14.14	4.960	[25]
Li_2CO_3+Co_3O_4+NiO, 500°C	2.854	14.135	4.953	[21]
LiOH+$Co(NO_3)_2$+$Ni(NO_3)_2$, 400°C	2.83	14.15	5.000	[26]
Li_2CO_3+$NiCO_3$+$CoCO_3$, 700/900°C	2.851	14.157	4.965	[27]
LiOH+NH_4 ascorbate, 350/700°C	–	–	–	[28]
$LiNO_3$+$Co(NO_3)_2$+$Ni(NO_3)_2$, 500/800°C	–	–	–	[29]

2. Experimental

The thermal decomposition behavior of the precursors was examined by means of thermogravimetry (TG) and differential thermal analysis (DTA) using a Netzsch analyzer (model STA 409) with simultaneous recording of weight losses (gravimetric thermal analysis) and temperature variations (differential scanning calorimetry). X-ray diffraction patterns were obtained with a Philips X-ray diffractometer (model PW1830) using nickel-filtered Cu Kα radiation (λ=1.5406 Å). The diffraction patterns were taken at room temperature in the range $10°<2\theta<80°$ using step scans. The step size and the scan rate were set at 0.1 and 0.2° min^{-1}, respectively. The particle morphology of the materials was examined by scanning electron microscopy (SEM, Cambridge Instruments, Stereoscan 120).

Fourier transform infrared (FTIR) absorption spectra were recorded at room temperature using a Brucker model IFS113v interferometer. The spectrometer was equipped with a 3.5-μm thick beamsplitter, a globar source, and a DTGS/PE far-infrared detector. Samples were ground to fine powders painted onto pellets of solid paraffin or polyethylene slabs. Data were collected in transmission mode at a spectral resolution of 2 cm^{-1} after 256 scans in vacuum atmosphere.

Electrochemical studies were carried out on the synthesized products annealed at 600°C in order to test their suitability as cathode-active material in high voltage lithium-containing batteries. The above tests were performed to measure quantitatively the capacity and cyclability of the synthesized product. The laboratory-scale Li//$LiNi_{0.5}Co_{0.5}O_2$ cells were fabricated employing a non-aqueous electrolyte prepared by dissolving 1 M $LiClO_4$ in propylene carbonate (PC). The typical composite cathode consisted of a mixture of $LiNi_{0.5}Co_{0.5}O_2$ powder, acetylene black and colloidal PTFE binder in 90:5:5 weight ratio. The PTFE-acetylene black was used to provide good electrical conductivity as well as mechanical toughness between active grains. The above mixture was pressed on to an expanded aluminium microgrid at a pressure of 500 MPa. This procedure yielded circular pellet electrodes of 10-mm diameter. The pellets were then dried at 120°C in air. Glass paper membrane was used as the separator between the cathode and the anode. Electrodes and separators were soaked in the electrolyte before being housed in a Teflon laboratory-cell hardware. In order to assess their electrochemical performance, galvanostatic charge–discharge cycles were recorded using a Mac-Pile system at a slow scan mode (i.e. current pulse of 0.1 mA cm^{-2} for 1 h followed by relaxation period of 0.5 h) in the potential range between 2.5 and 4.0 V. This procedure was used in order to record the quasi open-circuit voltage profiles of the lithium cells.

3. Sample preparations

The $LiNi_{0.5}Co_{0.5}O_2$ samples were synthesized using four low-temperature methods, which consisted of acidification of aqueous solutions of the starting salts. There are namely citric acid-acetate sol–gel, oxalic acid-acetate co-precipitation, glycine-nitrate combustion, and succinic acid-acetate pyrolysis process (Table 2). These techniques are based on the preparation of colloidal suspension, a sol, which turns into either a gel or a precipitate product. The products are further treated as shown on the general flow chart (Fig. 1) showing the steps used in the processing of lithium–nickel–cobalt oxide

powders. The LTOMs were grown from either acetates or nitrates via inorganic polymerization reactions in solution. Compared with the conventional powder route, they offer many advantages such as a lower temperature processing or better control of morphology of materials.

Table 2.

The various wet-chemistry methods used for the growth of $LiNi_{0.5}Co_{0.5}O_2$ powders

Method	Salt	Complexing agent	Molecular weight	Molecular formula
A	Acetates	Citric acid	192.43	$HOC(COOH)(CH_2COOH)_2$
B	Acetates	Oxalic acid	90.04	HOOCCOOH
C	Nitrates	Glycine	75.07	NH_2CH_2COOH
D	Acetates	Succinic acid	118.09	$HOOCCH_2CH_2COOH$

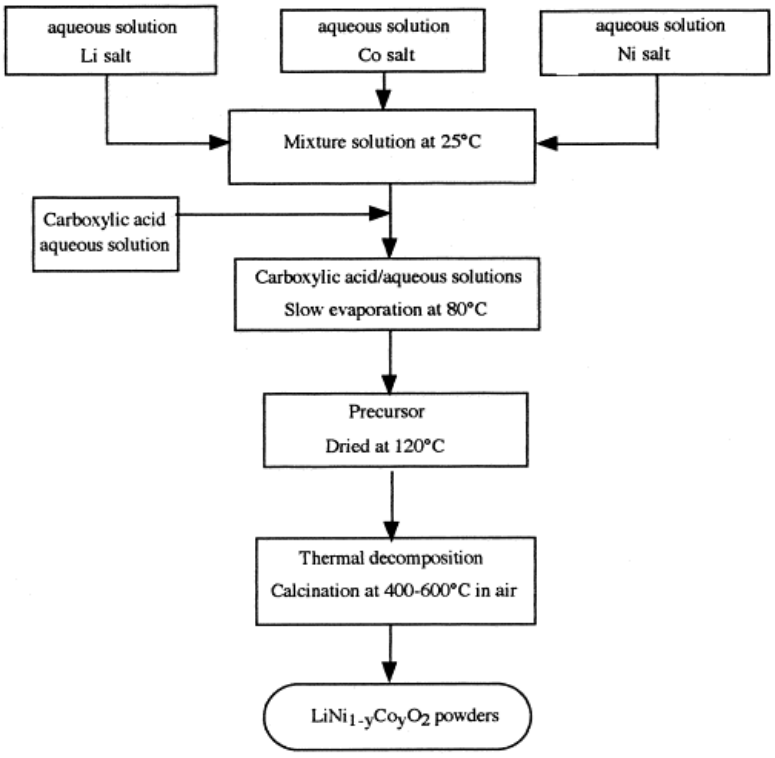

Fig. 1. Synthetic procedure of polycrystalline $LiNi_{0.5}Co_{0.5}O_2$ powders by the wet-chemistry techniques.

3.1. Citric acid-assisted method (A)

This method involves the mixing of acetates of the metals (Ni and Co) with the complexing agent, citric acid, in an aqueous medium. Stoichiometric amounts of

acetate hydrates of Li, Co and Ni (Fluka, purum p.a. grade) were dissolved in triple distilled water and thoroughly mixed with an aqueous solution of citric acid (Fluka, MicroSelect grade). Citric acid, $HOC(COOH)(CH_2COOH)_2$, was used as a chelating agent in making a gel. The resultant solution was then evaporated off at 80°C with magnetic stirring for about 6 h until a sol was formed. Heating the sol to moderate temperature causes a condensation reaction between □COOH groups via dehydration with the concurrent formation of water. As most of the excess water was removed, the sol turned into a gel, and extremely high viscosity resin was formed. The resulting xerogel turned into transparent violet color. Finally, the products referred to as precursor powders were formed by heating the violet-colored gel at 120°C. It is a fluffy brownish black powder. The decomposed powders were further heated to 400–700°C in air to obtain single-phase polycrystalline $LiNi_{0.5}Co_{0.5}O_2$ powders.

3.2. Oxalic-acid assisted method (B)

This synthesis procedure consists of preparing the mixture of acetates of the transition metals (Ni and Co) with $Li(COOCH_3)$ dissolved in triple distilled water and a solution of oxalic acid (dicarboxylic acid C_2:HOOCCOOH), in an aqueous medium. Oxalic acid acts as a precipitating agent. When all the above chemicals were mixed, a pink colored precipitate settled down from the pink colored solution. The resultant solution was then evaporated off at 80°C with magnetic stirring for about 6 h until a paste was formed. The resulting mass product (paste) turned transparent brownish black. Finally, the products referred to as precursor powders were formed by heating the paste at 120°C. The decomposed powders were slightly ground and further fired to 400–700°C in air to obtain single-phase $LiNi_{0.5}Co_{0.5}O_2$ powders. They were fluffy brownish black powders. The origin of the color change during this process is obviously due to oxidation of cations from divalent (Ni^{2+}/Co^{2+}) to trivalent state (Ni^{3+}/Co^{3+}).

3.3. Glycine-assisted method (C)

A stoichiometric amount of lithium and metal nitrate salts was dissolved in triple distilled water with a small proportion of ethanol and mixed with an aqueous solution of aminoacetic acid (glycine). Then this acidic solution was evaporated to dryness at 90°C for few hours. The rose-red colored solution turned to a violet colored gel, which decomposed by calcination to give an AA precursor. The slurries were heated at 400°C for few hours to get a product of the composition $LiNi_{0.5}Co_{0.5}O_2$. Glycine, NH_2CH_2COOH, acts as fuel, decomposes the homogeneous precipitate of metal complexes at low temperature, and yields the free impurity $LiNi_{0.5}Co_{0.5}O_2$ compound.

During this process the mass precursor darkened progressively as a result of oxidation. The origin of the color change during the firing process was obviously due to oxidation of divalent cations (Ni^{2+}, Co^{2+}) to trivalent cations (Ni^{3+}, Co^{3+}). The yield was a brownish-black powder with submicron-sized particles. Accordingly, the powder mass was fired at 600°C in air for 5 h to improve the crystallinity of $LiNi_{0.5}Co_{0.5}O_2$ final product. A theoretical reaction, assuming complete thermal decomposition of the starting materials, may be written as

$$LiNiO_3(aq) + (1-y)Ni(NO_3)_2(aq) + yCo(NO_3)_2 + 6NH_2CH_2COOH(aq) \ \Delta \text{ in air} \rightarrow LiNi_{1-y}Co_yO_2(s) + 2N_2(g) + 2CO_2(g) + 2CO(g) + 3H_2O(g),$$

which ultimately gave rise to a brownish black powder.

3.4. Succinic acid-assisted method (D)

Lithium and transition-metal acetates (reagent grades) were dissolved in a methanolic aqueous solution. An equal volume of a 1 mol dm^{-3} aqueous solution of succinic acid ($HOOCCH_2CH_2COOH$) was added as a complexing agent in the above methanolic or aqueous solution. In this case, care was exercised in adjusting the concentration of the complexing agent, the pH of the solution ranged between 3 and 4. Upon adding the above complexing agent, homogeneous precipitates were obtained, which were finely dispersed in the solution medium. It is believed that the carboxylic groups on the succinic acid form a chemical bond with the metal ions and these mixtures develop the extremely viscous paste-like substance upon slow evaporation of methanol and acetic acid. The paste was further dried at 120°C to obtain the dried precursor mass. The precursor was then allowed to decompose in air at around 290°C. Decomposition resulted in a huge exothermic reaction as exemplified by the combustion of organic species present in the precursor mass. This exothermic process, which yielded a brownish black colored powder, enhanced the oxidation reaction and onset the phase formation of the layered $LiNi_{0.5}Co_{0.5}O_2$ compound. During the heating sequence, the samples were maintained at each temperature for 4 h and then slowly cooled down to room temperature.

4. Results and discussion

4.1. Thermal analysis

Fig. 2A–D shows the TG–DTA curves, which display the formation temperature of the oxide $LiNi_{0.5}Co_{0.5}O_2$grown by the carboxyl acid-assisted aqueous methods. A strong exothermic peak appears in the range 200–350°C after the departure of the remaining water molecule at ca. 120°C. The formation temperature of the oxide prepared ranges from 300 to 400°C. The exothermic effect corresponds to the combustion of carboxylic acid and nitrate/acetate ions. More than half of the weight loss occurs during this stage because of a violent oxidation-decomposition reaction. During the combustion process, the solution turned into brownish black powder. Assuming that complexing agents provide combustion heat for calcination in the synthesis of oxide powders, it appeared that these carboxylic acids act as fuels during the pyrolysis of the precursor, accelerating the decomposition of nitrate/acetate ions in the process. Eventhough crystallization started below 400°C, well-crystallized and pure phases were obtained at 600°C. While pyrolysis procedures at this stage were very complicated, it could be presumed that the last weak exothermic peaks at ca. 380–398°C in the DTA curves of citric acid- and glycine-assisted methods correspond to the crystallization of the $LiNi_{0.5}Co_{0.5}O_2$ phase.

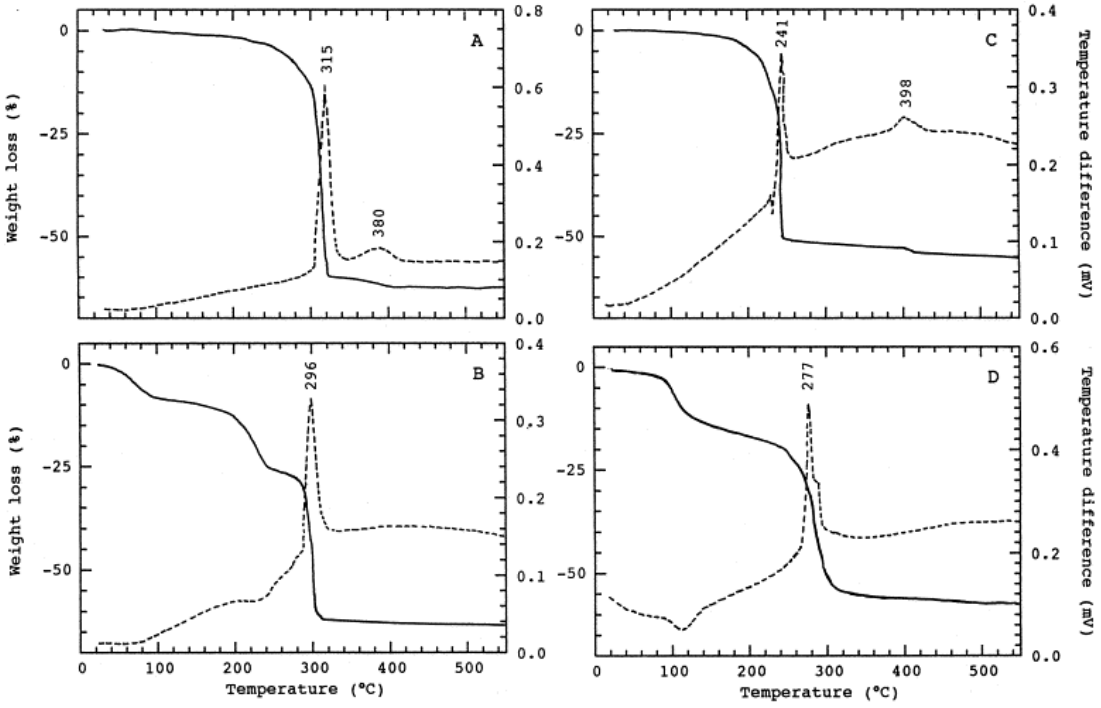

Fig. 2. TG–DTA curves of the $LiNi_{0.5}Co_{0.5}O_2$ grown by (A) the citric acid-assisted; (B) oxalic acid-assisted; (C) glycine-assisted; and (D) succinic acid-assisted wet-chemistry techniques.

These measurements were carried out at a heating rate of 10°C min^{-1} with oxygen flow.

4.2. Structure and morphology

X-ray diffraction analyses were carried out on the synthesized products at various preparation stages of $LiNi_{0.5}Co_{0.5}O_2$ powders to monitor the phase purity and structure, phase concentrations and the amorphous content. These preliminary results obtained from the precursors indicate that polycrystalline powders are grown with the tendency of a layered α-$NaFeO_2$ type structure. When a material was precalcined at 400°C, a significant amount of the $LiNi_{0.5}Co_{0.5}O_2$ phase peaks and a small amount of the impurity peaks were detected. This is quite consistent with the DTA data, which show the crystallization peak at 380–398°C.

Fig. 3A–D shows the X-ray diffraction patterns of microcrystalline $LiNi_{0.5}Co_{0.5}O_2$ powders grown by the various carboxylic acid-assisted methods. A single-phase $LiNi_{0.5}Co_{0.5}O_2$ with an α-$NaFeO_2$ type structure was grown when the precursors were calcined at 600°C. It took at least 5 h to attain full crystallinity. XRD peaks were indexed in the hexagonal system assuming $R\bar{3}m$ symmetry. It is assumed that lithium ions are in octahedral sites between $(Ni_{0.5}Co_{0.5}O_2)n$ infinite slabs formed by edge-sharing $(Ni_{0.5}Co_{0.5})O_2$ octahedra. Hexagonal cell parameters of the oxides prepared by four different methods, which were calculated by least-squares refinement, are given in Table 3. They are in good agreement with the reported values (seeTable 1). In all cases, the metal–metal intrasheet distance (a_{hex}=2.845±0.004 Å) was almost identical. Constructing the crystallographic $Ni_{0.5}Co_{0.5}O_2$ layers by substituting the sites of the Co^{3+} ions for the Ni^{3+}ions and calculating correspondingly the *c*/*a* value, one reveals that the hexagonal-close-packed lattice is still maintained, in other words, no cation mixing between the Ni^{3+} and Li^{+} ions present in octahedral sites if the *c*/*a* value is between 4.95. The sample particles are submicron-sized spherical grains, which are adequate for good electrochemical performance. However, $LiNi_{0.5}Co_{0.5}O_2$ powders grown by these wet-chemistry methods exhibit XRD patterns with well-defined doublets (006,102) and (108,110). The *c*/*a* ratio (Table 3) very different from the critical value 4.90 (cubic lattice) and the clear splitting of the (006) and (102) as well as (108) and (110) diffraction lines indicate that, as far as XRD patterns are concerned, an ordered distribution of lithium and transition-metal ions exists in the structure [30] and [31]. XRD results confirm the formation of pure phase, but the question of the local cationic order will be re-examined below by spectroscopic measurements.

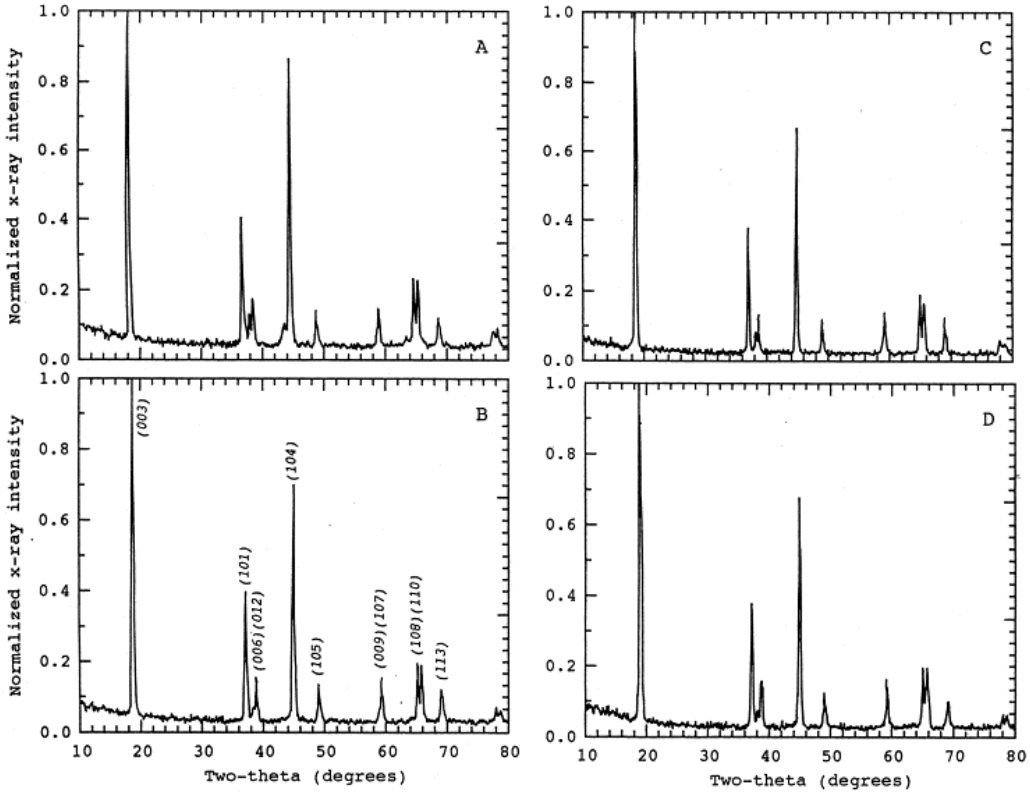

Fig. 3.

Observed XRD diagrams of microcrystalline $LiNi_{0.5}Co_{0.5}O_2$ powders calcined at 600°C. Powders were synthesized by (A) citric acid-assisted; (B) oxalic acid-assisted; (C) glycine-assisted; and (D) succinic acid-assisted wet-chemistry techniques. XRD peaks were indexed assuming the $R\bar{3}m$ symmetry (hexagonal).

Table 3.

XRD results obtained on $LiNi_{0.5}Co_{0.5}O_2$ powders calcined at 600°C[a]

Method of preparation	Lattice parameters			Unit-cell volume (Å^3)	R [b]
	a (Å)	*c* (Å)	*c*/*a*		
Citric acid	2.849	14.161	4.97	99.54	0.039
Oxalic acid	2.843	14.105	4.96	98.76	0.048
Glycine	2.841	14.113	4.97	98.66	0.012
Succinic acid	2.845	14.109	4.96	98.90	0.086

a The lattice parameters are given assuming the $R\bar{3}m$ symmetry (hexagonal).

b The reliability index *R* was calculated from $\sum |I_{obs} - I_{cal}| \ / \ \sum |I_{obs}|$.

4.3. Vibrational spectra

The purpose of this study was to investigate the local environment of cations in a cubic close-packed oxygen array of the $LiNi_{0.5}Co_{0.5}O_2$ lattice using FTIR spectroscopy. IR modes correspond to vibrations involving primarily atomic motion of cations against their oxygen neighbors. Consequently, these modes are very sensitive to the cationic local environment in the host matrix. Fig. 4A–D displays the FTIR spectra of synthesized $LiNi_{0.5}Co_{0.5}O_2$ samples fired at 600°C for 5 h. The FTIR absorption spectra display features, can be divided into two parts. (i) The high-wavenumber region of strong absorption corresponds to the broad rock-salt band which has broken into several distinct components at ca. 400–600 cm^{-1}, and (ii) the low-wavenumber region in which an isolated strong band is centered at ca. 240–260 cm^{-1}. The frequency of the vibrational modes and the analysis of the spectroscopic data of $LiNi_{0.5}Co_{0.5}O_2$ are summarized inTable 4. Effect of calcination is also clearly observed by FTIR measurements (Fig. 5). The FTIR spectrum of oxalic acid-synthesized $LiNi_{0.5}Co_{0.5}O_2$ samples fired at 400°C exhibited IR bands, which were due to impurities and disorder in the cationic sublattice.

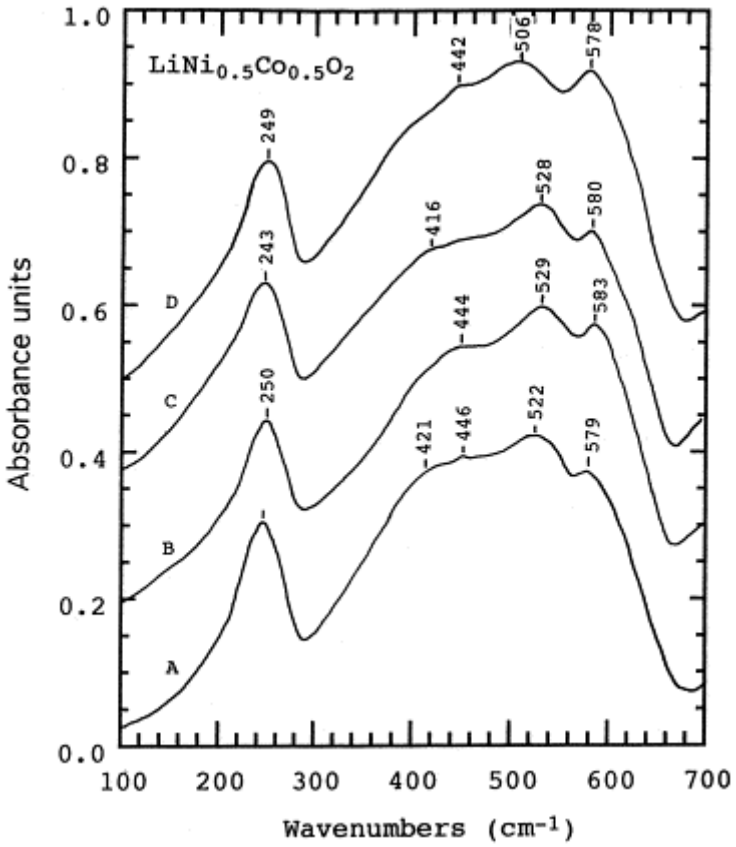

Fig. 4.
Typical room temperature FTIR absorption spectra of $LiNi_{0.5}Co_{0.5}O_2$ samples prepared by (A) citric acid-assisted; (B) oxalic acid-assisted; (C) glycine-assisted; and (D) succinic acid-assisted wet-chemistry techniques and calcined at 600°C.

Table 4.

Wavenumbers (in cm^{-1}) and assignments of the IR-active modes of the layered $LiNi_{0.5}Co_{0.5}O_2$ compounds

Mode	Frequency	Assignment
v_1	250	Stretching $v(LiO_6)$
v_2	444	Bending δ(O□M□O)
v_3	529	Bending δ(O□M□O)
v_4	582	Stretching $v(MO_6)$

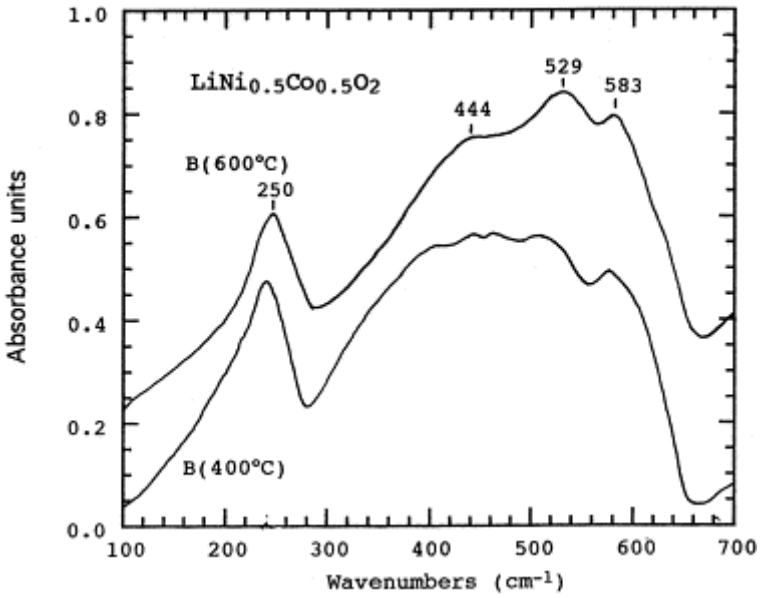

Fig. 5.
FTIR absorption spectra of $LiNi_{0.5}Co_{0.5}O_2$ samples prepared by the oxalic acid-assisted wet-chemistry techniques and calcined at (A) 400; and (B) 600°C for 5 h.

Layered oxides $LiMO_2$ possess a crystal structure consisting of alternating layers of trigonally distorted LiO_6 and MO_6 octahedra sharing edges. It has been shown that $LiNi_{1-y}Co_yO_2$ is a solid solution of $LiMO_2$(M=Ni, Co) compounds and that stoichiometric compounds belongs to crystallographic $R\bar{3}m$ space group. The transition-metal cations (i.e. cobalt and nickel) and the lithium ions are located at Wyckloff sites 3(a) and 3(b), respectively, in a cubic close-packed oxygen array. The Li^+ and Co^{3+}/Ni^{3+} ions are ordered along the (111) direction of the rock-salt cubic lattice leading to a two-dimensional structure. The IR modes of crystalline $LiNi_{1-y}Co_yO_2$ can be predicted by factor group analysis with a Bravais cell which contains one molecule (Z=1). The group factor analysis of the D_{3d}^5 spectroscopic symmetry yields four infrared-active modes [32]. Because FTIR spectroscopy is capable of probing directly the surrounding environment of the cation, we studied the local environment of lithium ions in $LiMO_2$ materials [33], [34] and [35]. It has also been demonstrated that the IR resonant

frequencies of alkali metal cations in their octahedral interstices in inorganic oxides are located in the frequency range 200–300 cm^{-1} [36]. Our recent work on transition-metal substitution in $LiMO_2$ compounds has shown that vibrational mode component of the LiO_6 octahedra appears invariably around 250 cm^{-1} [37]. Thus, the IR resonant frequency of LiO_6 groups appears at 269 and 234 cm^{-1} in the $LiCoO_2$ and LiNiO2 layered structures ($R\bar{3}m$ space group), respectively. As far as the low-wavenumber peak is concerned, the isotopic Li replacement in $LiMO_2$ has proven that this IR band between 200 and 300 cm^{-1} is associated with the vibration of a relatively isolated LiO_6 octahedron [38].

Thus, the IR absorption bands of $LiNi_{0.5}Co_{0.5}O_2$ microcrystalline powders are attributed as follows. The band situated at 250 cm^{-1} is assigned with confidence to an asymmetric stretching vibration of the Li^+ ion with O^{2-} near neighbors in $LiNi_{0.5}Co_{0.5}O_2$. However, a small mixing of Li□O stretching and O□M□O bending motion is present in the low-wavenumber peak. The high-frequency bands of the FTIR absorption spectra of $LiNi_{0.5}Co_{0.5}O_2$ located at ca. 583 cm^{-1} are attributed to the asymmetric stretching modes of MO_6group, whereas the low-frequency bands at ca. 444 and 529 cm^{-1} are assigned to the bending modes of O□M□O chemical bonds.

FTIR measurements confirm XRD data showing the formation of pure phase $LiNi_{0.5}Co_{0.5}O_2$. However, we got additional information on the lattice structure, especially on the distribution of the transition metal in the (Ni, Co)O_2 slabs. The shape of the FTIR spectra of the fired product (Fig. 4, curves B–D) shows the predominance of the high-wavenumber modes. The slight frequency shift of the bending modes in the FTIR spectrum of the sol–gel product compared with the combustion material leads to the cationic disorder in the $(Ni_{0.5}Co_{0.5})O_2$ slabs. The frequency shift of the LiO_6 mode has two origins, (i) the slight expansion of the interslab distance (c_{hex} cell parameter) in $LiNi_{0.5}Co_{0.5}O_2$ samples; and (ii) the small mixing of Li□O stretching and O□M□O bending motion present in the low-wavenumber peak.

The broadening of the high-wavenumber IR bands may be related with inhomogeneous Ni/Co distribution, variation in the cation–anion bond lengths, and/or polyhedral distortion occurring in $LiNi_{0.5}Co_{0.5}O_2$. It has been reported that the local distortion increases with the decrease of the cobalt concentration in the solid solution [35]. Recording ^7Li NMR spectra of $LiNi_{1-y}Co_yO_2$ compounds, Delmas et al. [39] and [40] have detected slight deviations from a homogeneous Ni/Co distribution and cobalt segregation in the $LiNi_{1-y}Co_yO_2$ solid solution. It seems that the predominance of the bands in medium-range frequency (at 421 and 446 cm^{-1}) of the IR

spectrum of sol–gel products (samples A) are due to a local disorder in the (Ni, Co)O_2 slabs, i.e. inhomogeneous Ni/Co distribution. These results show that FTIR of $LiNi_{0.5}Co_{0.5}O_2$materials permits the accurate detection of short scale heterogeneities complementing the X-ray diffraction analysis, which provides information only on the long-range structure.

4.4. Electrochemical studies

Electrochemical studies in lithium cells were carried out to compare the performance of low-temperature $LiNi_{0.5}Co_{0.5}O_2$ electrodes prepared by the different aqueous solution methods. Electrochemical properties were examined in lithium-containing test cells employing a non-aqueous electrolyte medium. The electrodes were separated by a porous membrane soaked in an electrolyte of 1 M $LiClO_4$ in PC. The voltage–composition curve of the each of the electrochemical cells using sol–gel and combustion synthesized cathodes is given in Fig. 6A–D. The Li//$LiNi_{0.5}Co_{0.5}O_2$ cells were charged and discharged at current densities of 0.1 mA cm^{-2}, while the voltage was monitored between 2.5 and 4.0 V using the galvanostatic mode of the MacPile battery tester. These experiments were carried out at low rates to emphasize the relationship between structure and electrochemistry.

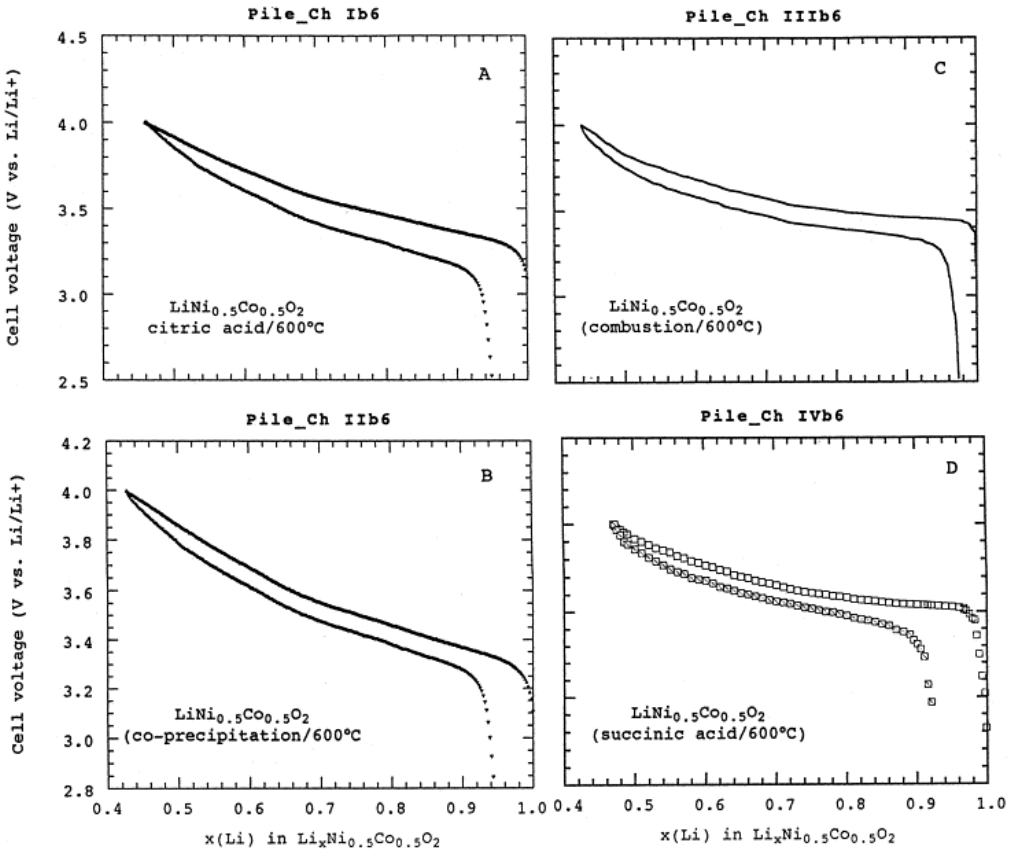

Fig. 6. Typical charge–discharge characteristics of Li//$LiNi_{0.5}Co_{0.5}O_2$ non-aqueous cell

employing the electrolyte of composition 1 M $LiClO_4$ in PC at room temperature. Charge and discharge were obtained at current density 0.1 mA cm^{-2}. $LiNi_{0.5}Co_{0.5}O_2$ cathode materials were calcined at 600°C and synthesized by the wet-chemistry techniques using (A) citric acid; (B) oxalic acid; (C) glycine; and (D) succinic acid.

In the potential domain 3.0–4.0 V, the charge–discharge curves correspond to the voltage profiles characteristic of the $Li_xNi_{0.5}Co_{0.5}O_2$ cathode materials associated with lithium occupation of octahedral sites, in agreement with previous works [16], [17], [18], [19], [20] and [21]. However, low-temperature synthesized $Li_xNi_{0.5}Co_{0.5}O_2$ cathode materials showed a lower potential for lithium deintercalation–intercalation than the materials prepared at high temperature, i.e. 800°C [26]. A similar behavior was also observed in the present investigation. The voltage profile of the cell with citric-assisted cathode exhibited a potential slightly lower than for glycine-assisted compound. This was due to the different crystallographic texture and morphology of these two materials. It was observed that the fully intercalated phase was not recovered during the first discharge. This was mainly due to the irreversible capacity loss because this capacity retention occurred also when the applied current density was decreased. It could be partially assigned to a kinetic problem especially as the phase $Li_xNi_{0.5}Co_{0.5}O_2$ is a poor electronic conductor. However, the polarization during both charge and discharge was almost similar in all cells. These studies also demonstrate that the D-cathode yields significantly inferior capacities (120 mAh g^{-1}) compared to other cathodes (130 mAh g^{-1}) when discharged to a cut-off voltage of 2.8 V (Fig. 6D). The improved performance of the Li//C□$Li_xNi_{0.5}Co_{0.5}O_2$ cell is evident (Fig. 6C) from the following factors, (i) the rate at which the capacity retention is lost during the first charge–discharge cycle is reduced; and (ii) the potential is superior in the entire length of charge–discharge. Actually, we do not have any consistent explanation for either the flat voltage or the higher starting potential of the Li//C□$Li_xNi_{0.5}Co_{0.5}O_2$ cell. Morphology or nanostructure could be at the origin of such a behavior.

The shape of the charge–discharge curves shows a good reversibility during the first cycle. In the composition domain $0.45 \leq x \leq 1.00$, the voltage charge profiles of the Li//$Li_xNi_{0.5}Co_{0.5}O_2$ cells exhibited an increase of the potential followed by a plateau at ca. 3.5 V. For $x<0.5$, the high voltage limit imposed in the experiments was rapidly reached. From the variation of the cell potential for the complete cells (Fig. 6A–D), one can distinguish the presence of two regions during the lithium insertion–extraction process. The voltage profiles exhibited a quasi-flat domain at about 3.5 V followed by a potential increase for a depth of charge $x<0.7$ and reached 4 V at $x=0.45$. The first

stage, near 3.5 V, was assigned to oxidation of Ni^{3+} ions as reported by Delmas et al. [19], [20] and [21]. In the initial composition region, the electrochemical charge curves (deintercalation process) were almost similar to those of the nickelate compound, while at x<0.5 the profiles were very close to that of the Li//Li$x$$CoO_2$ cell. Thus, the second stage (II), near 3.8 V, was attributed to oxidation of Co^{3+} ions. These evolutions came from the prior oxidation of Ni^{3+} ions before the cobalt ions.

The lithium extraction–insertion reactions in regions I and II proceeded in a Li$x$$Ni_{0.5}Co_{0.5}O_2$ matrix having a rhombohedral symmetry. Considering the fully charge state (at 4 V, x=0.45), we formulated the reaction in a Li//$LiNi_{0.5}Co_{0.5}O_2$ intercalation cell as

$$[Li_{0.45}Ni_{0.55}]_{3b}[Ni^{4+}_{0.5}\,Co^{4+}_{0.05}\,Co^{3+}_{0.45}]_{3a}[O_2]_{6c} + 0.55Li^{+} + 0.55e^{-} \leftrightarrow LiNi_{0.5}Co_{0.5}O_2,$$

in which 3a, 3b, and 6c is the number of equivalent positions combined in a space group $R\bar{3}m$ to represent the sites for each species. From this formulation theoretical capacity is calculated to be 273 mAh g^{-1}. In Eq. (2), the ratio Co^{4+}/Ni^{4+} could be determined by precise electrochemical titration assuming an ideal Faradaic process. The layered $LiNi_{0.5}Co_{0.5}O_2$ framework provides a two-dimensional interstitial space for rapid lithium intercalation and deintercalation. It is believed that the c-axis of the layered materials expands rapidly on delithiation due to a decrease of the electrostatic binding energy of the lithium-depleted layers [15]. As a concluding remark, it can be pointed out that low-temperature cathode materials exhibit acceptable electrochemical capacity with lower oxidation potential. These compounds are candidates to treat problems due to nickel dioxide formation and electrolyte degradation. This shows the advantage of the wet-chemistry synthesis method for $LiNi_{0.5}Co_{0.5}O_2$ preparation, since materials having similar properties can be elaborated in shorter time to reduce the cost of cathode materials. The electrochemical properties of $LiNi_{0.5}Co_{0.5}O_2$ cathode materials are presently being studied for long term cycling.

5. Conclusion

This work has shown that $LiNi_{0.5}Co_{0.5}O_2$ single phases are grown at low temperature using various aqueous solution techniques based on carboxylic acids. The low-temperature methods, in which carboxylic acids act as fuels and provide submicron-sized particles which are adequate for fast lithium intercalation–deintercalation reactions occurring in rechargeable lithium cells. The use of solution processing leads to molecular level mixing and highly uniform materials. The wet-chemistry techniques adopted for the synthesis of $LiNi_{0.5}Co_{0.5}O_2$ cathode materials have yielded particles, which favor good electrochemical performance. The charge–discharge voltage profiles of Li//Li$x$$Ni_{0.5}Co_{0.5}O_2$ cells show evolutions, which come from the prior oxidation of Ni^{3+} ions before the cobalt ions. These studies also demonstrated that the combustion synthesized-cathodes yield capacities in the range 120–130 mAh g^{-1}compared with the theoretical value 150 mAh g^{-1} when discharged to a cut-off voltage of 2.8 V ($1.0 \geq x \geq 0.45$). The good performance of the Li//Li$x$$Ni_{0.5}Co_{0.5}O_2$ cells using cathodes prepared by the aminoacetic acid-assisted method has been evidenced.

Acknowledgements

This work was partially supported by the Indo-French Centre for the Promotion of Advanced Research (IFCPAR) under Grant No. 1408-2.

References

1. P. Barboux, J.M. Tarascon, F.K. Shokoohi
   J. Solid State Chem., 94 (1991), p. 185

2. E. Rossen, J.N. Reimers, J.R. Dahn
   Solid State Ionics, 62 (1993), p. 53

3. T. Tsumura, A. Shimizu, M. Inagaki
   J. Mater. Chem., 3 (1993), p. 995

4. B. Garcia, P. Barboux, F. Ribot, A. Kahn-Harari, L. Mazerolles, N. Baffier
   Solid State Ionics, 80 (1995), p. 111

5. S.R.S. Prabaharan, M.S. Michael, T.P. Kumar, A. Mani, K. Athinarayanswamy, R. Gangadharan
   J. Mater. Chem., 5 (1995), p. 1035

6. B. Garcia, J. Farcy, J.P. Pereira-Ramos, J. Prichon, N. Baffier
J. Power Sources, 54 (1995), p. 373

7. W. Liu, G.C. Farrington, F. Chaput, B. Dunn
J. Electrochem. Soc., 143 (1996), p. 879

8. I.-H. Oh, S.-A. Hong, Y.-K. Sun
J. Mater. Sci., 32 (1997), p. 3177

9. J.P. Pereira-Ramos
J. Power Sources, 54 (1995), p. 120

10. K. Mizushima, P.C. Jones, J.B. Goodenough
Mater. Res. Bull., 15 (1980), p. 763

11. T. Nagaura, Paper presented at the 4th International Rechargeable Battery Seminar, Deerfield Beach, FL, March 1990.

12. J.R. Dahn, U. von Sacken, R. Fong, Primary and Secondary Batteries Symposium, 178th Electrochem. Soc. Meeting, Seattle, WA, 10–14 October, 1990.

13. Y. Nishi, H. Azuma, A. Omaru, US Patent 4,959,281, 1990.

14. T. Nagaura, K. Tozawa
Prog. Batt. Solar Cells, 9 (1990), p. 209

15. R.J. Gummow, M.M. Tackeray
Solid State Ionics, 53–56 (1992), p. 681

16. C. Delmas, I. Saadoune
Solid State Ionics, 53–56 (1992), p. 370

17. T. Ohzuku, A. Ueda, M. Nagayama, Y. Iwakoshi, H. Komori
Electrochim. Acta, 38 (1993), p. 1159

18. E. Zhecheva, R. Stoyanova
Solid State Ionics, 66 (1993), p. 143

19. A. Rougier, I. Saadoune, P. Gravereau, P. Willmann, C. Delmas
Solid State Ionics, 90 (1996), p. 63

20. C. Delmas, I. Saadoune, A. Rougier
J. Power Sources, 43–44 (1993), p. 595

21. I. Saadoune, C. Delmas
J. Mater. Chem., 6 (1996), p. 193

22. T. Ohzuku, H. Konori, K. Sawai, T. Hirai
Chem. Express, 5 (1990), p. 733

23. T. Ohzuku, T. Hirai, Extended Abstracts of 6th Lithium Batteries Meeting, Munster, 1992, Abstr. FRI-04, p. 139.

24. A. Ueda, T. Ohzuku
J. Electrochem. Soc., 141 (1994), p. 2010

25. S.J. Lee, J.K. Lee, D.W. Jim, H.K. Baik
J. Electrochem. Soc., 143 (1996), p. L268

26. D. Caurant, N. Baffier, B. Garcia, J.P. Pereira-Ramos
Solid State Ionics, 91 (1996), p. 45

27. Y.M. Choi, S.I. Pyun, S.I. Moon
Solid State Ionics, 89 (1996), p. 43

28. F. Croce, A. Deptula, W. Lada, R. Marassi, T. Olczak, F. Ronci
Ionics, 3 (1997), p. 390

29. Y.K. Sun, I.H. Oh, K.Y. Kim
J. Mater. Chem., 7 (1997), p. 1481

30. J. Morales, C. Perez-Vicente, J.L. Tirado
Mater. Res. Bull., 25 (1990), p. 623

31. J.R. Dahn, U. von Sacken, C.A. Michael
Solid State Ionics, 44 (1990), p. 87

32. R.K. Moore, W.B. White
J. Am. Ceram. Soc., 53 (1970), p. 679

33. C. Julien, A. Rougier, G.A. Nazri
Mater. Res. Soc. Symp. Proc., 453 (1997), p. 647

34. A. Rougier, G.A. Nazri, C. Julien
Ionics, 3 (1997), p. 170

35. M. Nazri, D. Curtis, B. Yebka, G.A. Nazri, C. Julien, Extended Abstracts of 193th Meeting of the Electrochem. Soc., vol. 98-1, San Diego, CA, 3–8 May, 1998.

36. G.J. Exarhos, W.N. Risen
Solid State Commun., 11 (1970), p. 755

37. C. Julien, M. Massot, C. Perez-Vicente, E. Haro-Poniatowski, G.A. Nazri, A. Rougier
Mater. Res. Soc. Symp. Proc., 496 (1998), p. 415

38. P. Tarte, J. Preudhomme
Spectrochim. Acta, 26A (1970), p. 747

39. C. Marichal, J. Hirschinger, P. Granger, M. Menetrier, A. Rougier, C. Delmas
Inorg. Chem., 34 (1995), p. 1773

40. M. Menetrier, A. Rougier, C. Delmas
Solid State Commun., 90 (1994), p. 439

Corresponding author. Tel.: +33-144-274561; fax: +33-144-274512